ACS OMEGA

Open Access

http://pubs.acs.org/journal/acsodf

Article

Amino Acid-Driven Dimensional Reduction of $CsPbBr_3$ Nanocrystals

Nikunj Agarwal,[§] Deepshikha Agarwal,[§] and Tushar Debnath*

Cite This: *ACS Omega* 2024, 9, 31026−31034

Read Online

ACCESS | Metrics & More | Article Recommendations | Supporting Information

ABSTRACT: Inspired by biomineralization, the recent incorporation of organic molecules into inorganic lattices shows interesting optical properties and tunability. We functionalize all inorganic $CsPbBr_3$ perovskite nanocrystals (PNCs) with amino acid (AA) cysteine using the water-hexane interfacial approach. Along with the AA cysteine, we added $AuBr_3$ salt into the aqueous phase, leading to the formation of a Au-cysteine thiolate complex to activate the aqueous to nonaqueous phase transportation of the AA via a molecular shuttle, oleylamine. The interaction between $CsPbBr_3$ PNCs and the Au-cysteine thiolate complex is probed using optical spectroscopy, which reveals dimensional reduction of the parent PNCs to form $CsPbBr_3$ nanoplatelets (NPls) and subsequent phase transformation to $CsPb_2Br_5$ NPls. X-ray diffraction, X-ray photoelectron spectroscopy, and high-resolution transmission electron microscopy conclusively support the above chemical transformation reaction via interfacial chemistry. We propose a mechanistic insight into the dimensional growth in one direction in the presence of AAs via preferential ligand binding to specific facets, leading to transformation from 3D cubes to 2D NPls, while, presumably, the phase transformation occurs via the CsBr stripping mechanism upon prolonged interaction with water. Since AAs are building blocks for several redox-active complex biological moieties, including proteins, investigation of the interaction of AAs with PNCs may be advantageous since the latter can act as a fluorescent probe for bioimaging application.

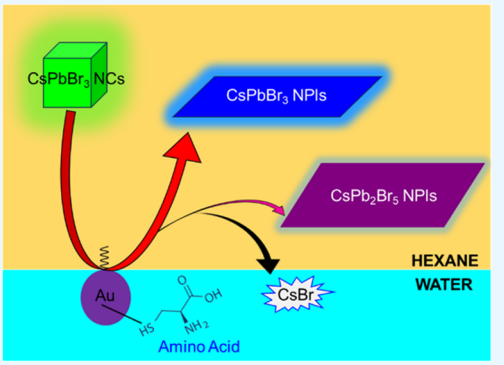

INTRODUCTION

To enhance the functionality of a semiconductor crystal, tuning its optical properties is essential, eventually allowing us to use them for a broad range of applications.[1,2] One can tune the optical properties by changing the band gap of the semiconductor material, e.g., by varying the size, composition, and doping.[3−5] Changing the dimension (e.g., 3D to 2D) is also another important means to tune the optical band gap without changing the composition.[6,7] Chemical transformation of a semiconductor to a different phase may also lead to optical property tunability.[8,9] Recently, inspired by biomineralization, manipulation of the band gap via incorporation of organic molecules in the inorganic lattice has emerged.[10−14] For example, semiconductors ZnO and Cu_2O exhibit substantial band gap opening in the presence of amino acids (AA), and the magnitude of the band gap opening is dependent on the AA concentration.[15−18] The inhomogeneous distribution of the AA within those semiconductors results in the introduction of the confinement effect, leading to a blue shift in the optical spectra due to band gap opening.[16,18] It is important to note that AAs are the building blocks of the complex biological system; therefore, unraveling the interaction between AA and semiconductors and their consequences on the optical properties may be advantageous for the use of semiconductors in bioimaging.

In this work, we functionalize $CsPbBr_3$ perovskite nanocrystals (PNCs) with AA cysteine to manipulate the optical properties of the $CsPbBr_3$ PNCs. While recently, AA incorporation in different semiconductor materials has attracted researchers, their incorporation in perovskites is rare.[19−21] Halide PNCs are a recent entrant in the semiconductor community due to their excellent optoelectronic properties, enabling them to be used in photovoltaic, light-emitting devices, etc.[22−26] The halide PNCs are surface functionalized with long-chain fatty acid ligands, e.g., oleic acid (OA), oleylamine (OLA), which are essential for their colloidal stability.[22,27] Importantly, the choice of ligands is crucial for controlling the size, shape, and morphology of PNCs, eventually governing the optical tunability.[28] Recent work on PNCs using zwitterionic ligands (lecithin) shows enhanced surface interaction, causing precise control over the size of the NCs.[29] AAs, on the other hand, exhibit zwitterionic characteristics and therefore may establish strong surface coupling with the PNCs. Early work shows that functionalization of PNCs with small molecules is advantageous in opening charge (electron) and energy transfer pathways, eventually beneficial for solar energy harvesting.[30−33] Similarly, AA

Received: May 8, 2024
Revised: June 5, 2024
Accepted: June 17, 2024
Published: July 1, 2024

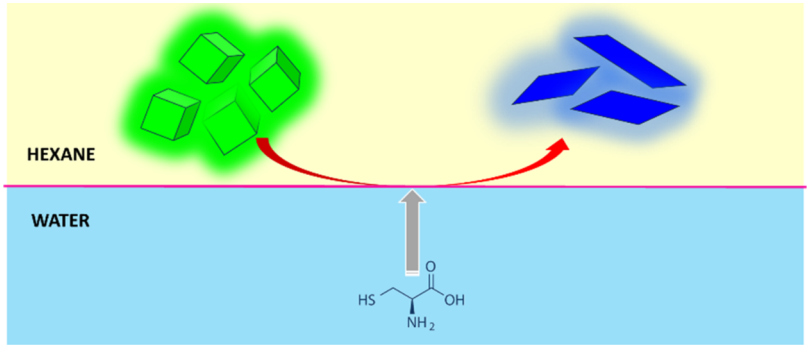

Figure 1. Schematic illustration showing the chemical transformation of green-emitting 3D cubic $CsPbBr_3$ NCs to blue-emitting 2D nanoplatelets in the presence of amino acid (AA) cysteine in the water-hexane interface.

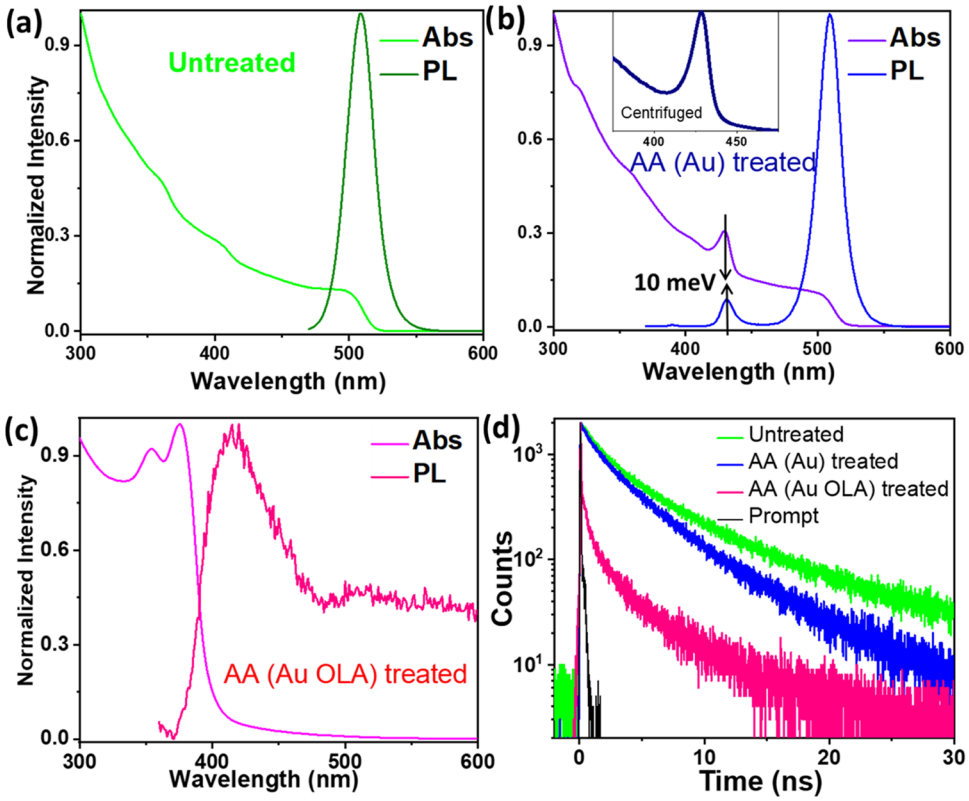

Figure 2. Optical absorption and PL spectra of (a) the untreated, (b) AA (Au)-treated, and (c) AA (Au-OLA)-treated $CsPbBr_3$ PNCs. (Inset b) The corresponding AA (Au)-treated PNCs after centrifugation, showing pronounced absorption resonance due to thin $CsPbBr_3$ NPls. (d) Time-resolved PL decay traces of the corresponding PNCs.

functionalization in PNCs may lead to shaping of their optical properties, which remains elusive to date.

In particular, we functionalized $CsPbBr_3$ PNCs with AA cysteine using a water-hexane interfacial strategy where the AA cysteine comes from the aqueous phase. In this water-hexane interfacial strategy, the surface-capped OLA ligands from $CsPbBr_3$ PNCs act as a molecular shuttle that transports molecules from the aqueous to the nonaqueous phase. To facilitate the molecular shuttling, in addition to AA cysteine, we added $AuBr_3$ salt in the aqueous phase, which resulted in the formation of a Au-cysteine thiolate complex. The complex then travels from water to the hexane phase via the OLA molecule, leading to the chemical transformation of $CsPbBr_3$ PNCs to the corresponding nanoplatelets (NPls), and finally to $CsPb_2Br_5$ NPls, both of which are decorated with Au particles. Blue-shifted optical absorption and photoluminescence (PL) spectra support the formation of $CsPbBr_3$ NPls, which further shifted to the UV region for $CsPb_2Br_5$ NPls. We performed X-ray diffraction (XRD), X-ray photoelectron spectroscopy (XPS), Fourier transform infrared (FTIR) spectroscopy, and high-resolution transmission electron microscopy (HRTEM) to support their formation. Finally, we provided a mechanism for the dimensional reduction and phase transformation of the $CsPbBr_3$ PNCs upon interaction with the Au-cysteine thiolate complex at the water-hexane interface. The interfacial chemical transformation reaction of PNCs using AA may find promising applications for the development of new materials with tunable optical properties.

RESULTS AND DISCUSSION

We functionalized halide PNCs with AA cysteine at the water-hexane interface, where the AA comes from an aqueous

https://doi.org/10.1021/acsomega.4c04364
ACS Omega 2024, 9, 31026−31034

solution, while the PNCs stay in hexane (Figure 1). To this end, we first prepared colloidal $CsPbBr_3$ PNCs using our earlier recipe, containing both oleic acid (OA) and oleylamine (OLA) as ligands, which show intense green PL under UV light, having ∼80% PL quantum yield (PLQY).[30] On treating the hexane solution of $CsPbBr_3$ PNCs with the AA-saturated aqueous solution in the presence of Au, the green PL turns into a weak blue PL, as shown in Figure 1. The detailed synthesis procedure of AA-functionalized PNCs is described in the Experimental Methods section. A drastic blue shift of ∼820 meV in the absorption spectra is observed, as will be revealed later, which indicates a structural or morphological change, or introduction of a strong quantum confinement effect.[18,34,35] Earlier, a blue shift in the optical absorption spectra was observed upon AA incorporation in semiconductor materials, which was correlated with the quantum confinement effect, where the magnitude of the blue shift (∼300 meV) was smaller.[16,18] Recently, the water-hexane interfacial strategy has been employed on a few occasions for chemical transformation of PNCs.[9,36−39] In our recent works, we have shown that transportation of metal salts from the aqueous to nonaqueous phase leads to formation of doped or hybrid PNCs.[40−42] Similarly, the AA cysteine may travel from the aqueous to the hexane phase to incorporate into PNCs, leading to AA functionalization on the PNCs. To understand the effect of the AA cysteine on the $CsPbBr_3$ PNCs along with the transport process from the aqueous to the hexane phase, we carried out detailed optical and morphological measurements, as discussed in the subsequent sections.

Figure 2a shows the optical absorption and PL spectra of untreated $CsPbBr_3$ PNCs. The optical absorption spectrum shows an exciton absorption at 500 nm and a PL maximum at 510 nm. On treating the PNCs with AA cysteine-saturated aqueous solution, an additional blue PL appears at 450 nm, however, without any corresponding/clear signature in the absorption spectrum (Figure S1). The blue PL at 450 nm indicates a morphological change or introduction of a quantum confinement effect,[18,34,35] possibly due to AA cysteine functionalization in $CsPbBr_3$ PNCs. Since we have not observed corresponding/clear changes in the absorption spectrum, the AA transportation from water to hexane might not be enough to induce corresponding changes in the absorption spectrum. This is possibly due to weak or no interaction between the shuttling ligand OLA and the AA cysteine, unlike our recently reported strong interaction of OLA with metal (e.g., Mn, Au) salts.[41,42]

Since cysteine makes strong interactions with Au atoms via the S end, to activate the interaction between the shuttling ligand OLA and AA cysteine and to initiate the cysteine transportation from water to the hexane phase, we added $AuBr_3$ salt in the aqueous solution in addition to the AA cysteine (hereafter, AA (Au)-treated PNCs). The corresponding optical absorption and PL spectra of the AA (Au)-treated PNCs are shown in Figure 2b. In addition to the broad exciton absorption at 500 nm, similar to that of the untreated $CsPbBr_3$ PNCs, a sharp and pronounced strongly blue-shifted (∼410 meV) absorption resonance is observed at 429 nm. Similarly, along with a strong PL at 510 nm from the untreated $CsPbBr_3$ PNCs, a new blue-shifted PL at 431 nm is observed with an overall PLQY of ∼9%. It is important to note that the new blue-shifted absorption resonance and PL have only a 2 nm Stokes shift compared to the ∼10 nm Stokes shift in the untreated PNCs. Earlier, a sharp and pronounced absorption resonance in a similar spectral position along with a significantly smaller Stokes shift was observed in thin (2-monolayer) $CsPbBr_3$ NPls.[41,43−45] This led us to hypothesize that on treating with AA (Au) aqueous solution, parts of the $CsPbBr_3$ PNCs chemically transform into thin $CsPbBr_3$ NPls having blue-shifted optical spectra due to the quantum confinement effect, where the AA cysteine plays an important role, which we will reveal later in this report. Here the obtained NPls show a quantum confinement effect as the width of the NPls (=4.5 nm, see later) is much smaller than the exciton Bohr radius of $CsPbBr_3$ (=7 nm). In effect, we observed mixtures of $CsPbBr_3$ nanocubes and NPls, both of which contribute to the optical spectra and can be separated via centrifugation (inset in Figure 2b).

To further increase the AA cysteine transportation from the aqueous to hexane phase, we added excess OLA ligand in the hexane phase to enhance the shuttling effect. The optical absorption and PL spectra of the resulting AA (Au-OLA)-treated PNCs are shown in Figure 2c. Surprisingly, the optical features of the untreated $CsPbBr_3$ PNCs disappear completely, and an entirely new optical behavior can be observed in the AA (Au-OLA)-treated PNCs, which are further blue-shifted from the AA (Au)-treated PNCs. The observation suggests that an even stronger morphology evolution of the parent $CsPbBr_3$ PNCs via AA cysteine functionalization has occurred. A strong absorption resonance at 375 nm, along with a shoulder at 355 nm, is observed in the absorption spectrum. The corresponding PL spectrum shows an extremely weak (PLQY < 0.1%) but clear broad PL between 380−500 nm, with a peak maximum at 415 nm. The emergence of the stark blue-shifted optical spectra indicates that a new morphology evolution has taken place upon AA cysteine functionalization via the chemical transformation of $CsPbBr_3$ PNCs, which we identified as the $CsPb_2Br_5$ phase. Earlier Zhang et al. synthesized $CsPb_2Br_5$, which has optical absorption and PL in the UV region, like ours.[46] A few other groups also reported the optical spectra of the $CsPb_2Br_5$ phase in a similar region, further strengthening our claim of formation of the $CsPb_2Br_5$ phase.[47,48] To emphasize the generality of this chemical transformation approach, we investigated the interaction of $CsPbBr_3$ PNCs with other AAs, e.g., threonine, and the corresponding absorption and PL spectra are shown in Figure S2. Similar to cysteine-treated $CsPbBr_3$ PNCs, both the absorption and PL spectra of the threonine-treated $CsPbBr_3$ PNCs depict a strong blue shift, directing the formation of $CsPb_2Br_5$ NCs.

To understand the excited-state dynamics of the untreated and AA-treated $CsPbBr_3$ PNCs, we performed time-resolved PL measurements upon 374 nm pulse laser excitation. Figure 2d shows the time-resolved PL decay traces of the untreated, AA (Au)-treated, and AA (Au-OLA)-treated $CsPbBr_3$ PNCs. The time-resolved PL decay trace of the untreated $CsPbBr_3$ PNCs can be fitted biexponentially, with 1.4 and 6.3 ns components, having an average excited-state lifetime of ∼3.7 ns (Table S1). The AA (Au)-treated PNCs, which later we identified as thin $CsPbBr_3$ NPls, show a slightly faster PL decay ($\tau 1$ = 1.17 ns and $\tau 2$ = 4.5 ns), having an average excited-state lifetime of ∼3 ns. The excited-state lifetime reduces drastically with a major fast 0.3 ns and a minor slow 3.3 ns component (τ_{avg} ∼ 0.74 ns) in the AA (Au-OLA)-treated PNCs, corresponding to $CsPb_2Br_5$ PNCs. The 0.3 ns component is consistent with the fast direct to indirect nonradiative process, while the slow component is the charge carrier recombination in this indirect semiconductor.

https://doi.org/10.1021/acsomega.4c04364
ACS Omega 2024, 9, 31026−31034

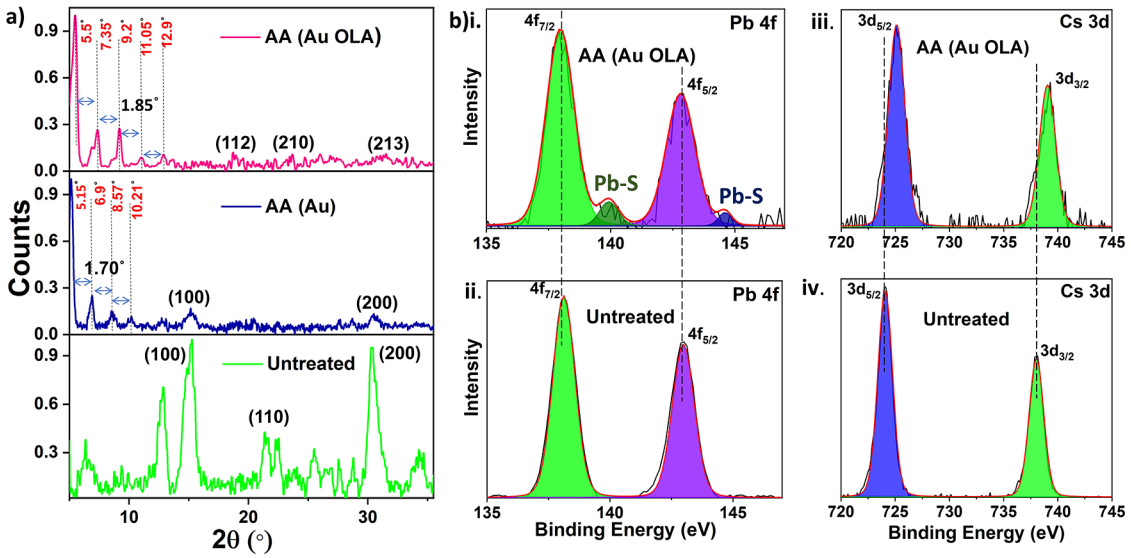

Figure 3. (a) XRD pattern of the untreated, AA (Au) treated, and AA (Au-OLA) treated $CsPbBr_3$ PNCs. (b) High-resolution XPS spectra of (i), (ii) Pb 4f and (iii), (iv) Cs 3d peaks of AA (Au-OLA) treated and untreated $CsPbBr_3$ PNCs, respectively.

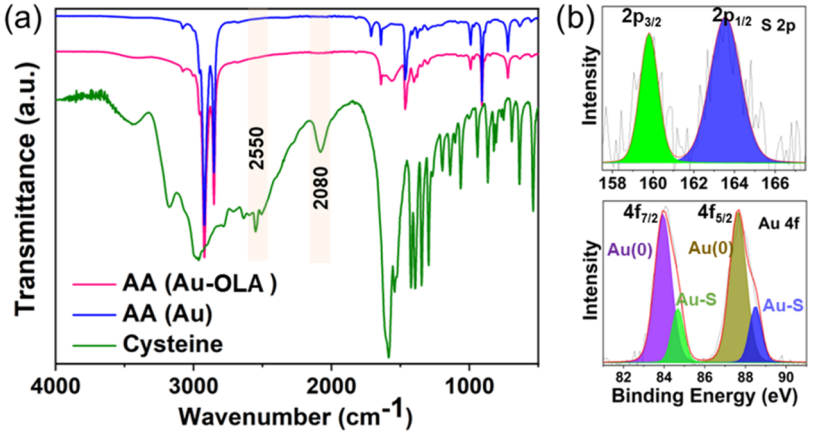

Figure 4. (a) FTIR spectra of cysteine, AA (Au)-treated, and AA (Au-OLA)-treated $CsPbBr_3$ PNCs. The shaded regions indicate two characteristic peaks of cysteine due to S−H and N−H vibrations. (b) High-resolution XPS spectra of S 2p and Au 4f of AA (Au-OLA)-treated $CsPbBr_3$ PNCs.

Further investigation of the structure, bonding, and morphology of the untreated and AA-treated PNCs was carried out using XRD, XPS, FTIR, and TEM measurements. The XRD pattern of the untreated PNCs shows diffraction peaks at 2θ = 15, 22, and 30°, corresponding to (100), (110), and (200) planes, respectively. The XRD pattern of the AA (Au)-treated PNCs shows a series of diffraction peaks in the low-angle region, along with the diffraction peaks at 2θ = 15 and 30° for $CsPbBr_3$ crystal. The series of diffraction peaks in the low-angle XRD was earlier referred to as the reflections from stacked NPls.[41,49] Combining pronounced absorption resonance and blue-shifted optical spectra along with the series of low-angle diffractions in XRD measurement strengthens our claim of the formation of $CsPbBr_3$ NPls upon AA (Au) treatment. Similarly, the XRD pattern of the AA (Au-OLA)-treated PNCs shows a few characteristic peaks of $CsPb_2Br_5$, e.g., (112), (210), and (213), along with a series of diffraction peaks in the low-angle region, corresponding to stacked $CsPb_2Br_5$ NPls. Moreover, we perform XPS measurements for the untreated and AA (Au-OLA)-treated $CsPbBr_3$ PNCs, and the corresponding high-resolution spectra for Pb 4f and Cs 3d peaks are shown in Figure 3b. Although no clear shift is observed in the main Pb 4f peaks, a clear shift to higher energy is observed in the Cs 3d peaks from untreated to AA (Au-OLA)-treated $CsPbBr_3$ PNCs, supporting electron-deficient $CsPb_2Br_5$ formation.

To shed light on the bonding of AA cysteine to perovskites, we performed FTIR measurement of cysteine, untreated, and AA cysteine-treated PNCs, i.e., AA (Au)- and AA (Au-OLA)-treated samples (Figures 4a and S3). The cysteine FTIR spectrum is characterized by an absorption peak at 2550 cm^{-1} due to S−H stretching vibrations and another at 2080 cm^{-1} due to N−H stretching vibrations (Figure 4a).[50] Upon treating the PNCs with AA (Au) and AA (Au-OLA), both absorption features disappear. This observation directs cleavage of the S−H bonds to form the Pb−S/Au-S bond, as well as the basification of the NH_3^+ group of the cysteine takes place during the synthesis.[50] Thus, we may conclude that the phase transition is indeed caused by the AA cysteine.

We further investigated the high-resolution XPS measurements of AA (Au-OLA)-treated $CsPbBr_3$ PNCs to unravel the presence of S and Au in the product. The core-level XPS spectra of S $2p_{1/2}$ and $2p_{3/2}$ of the corresponding sample show peaks at 163.6 and 159.8 eV, respectively, directing the

https://doi.org/10.1021/acsomega.4c04364
ACS Omega 2024, 9, 31026−31034

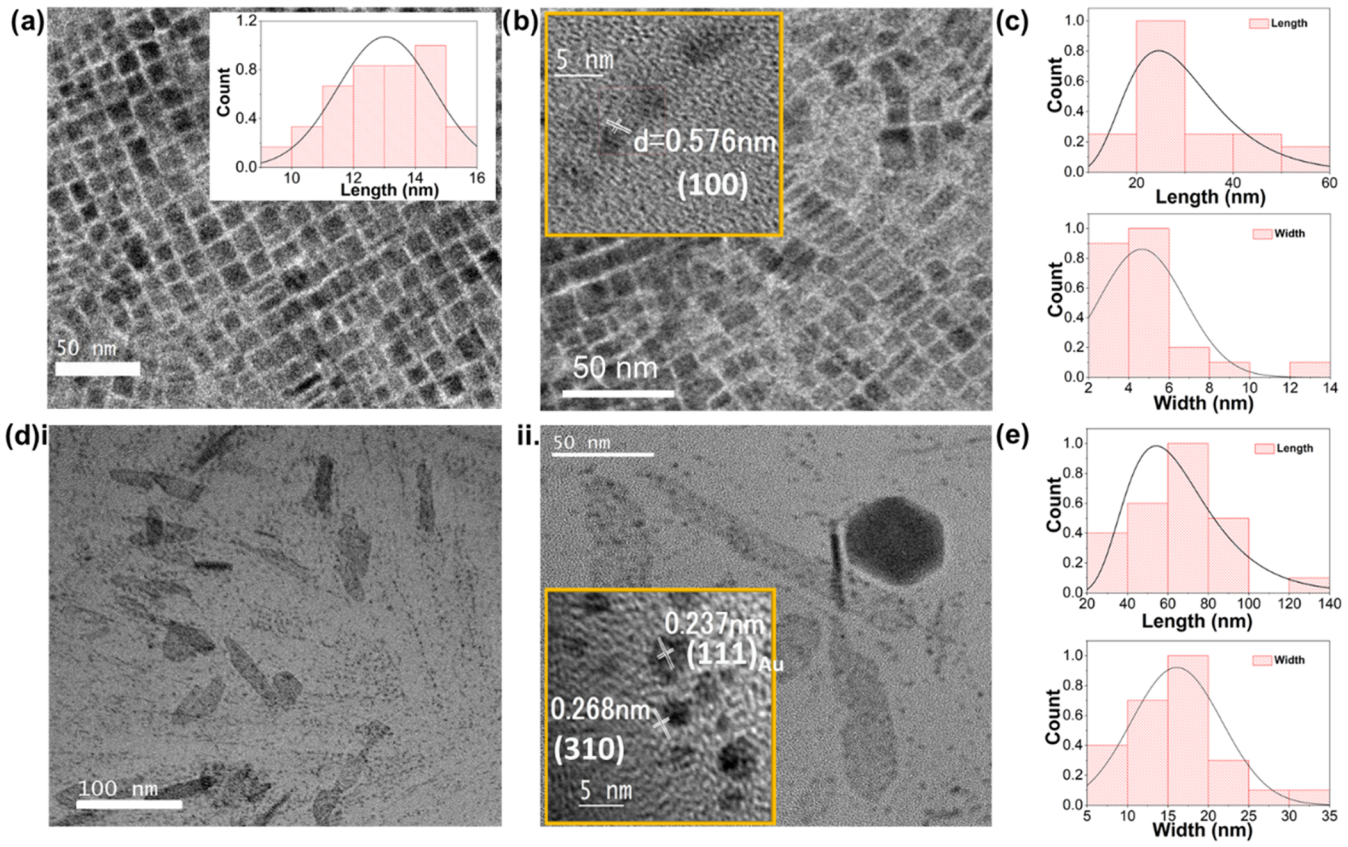

Figure 5. TEM images of (a) the untreated, (b) AA (Au)-treated, and (d) AA (Au-OLA)-treated $CsPbBr_3$ PNCs. Insets in (a) size distribution and (b, d) HRTEM images of the corresponding PNCs. (c, e) Size distribution along the length and width of the obtained nanoplatelets upon AA (Au) treatment and AA (Au-OLA) treatment, respectively.

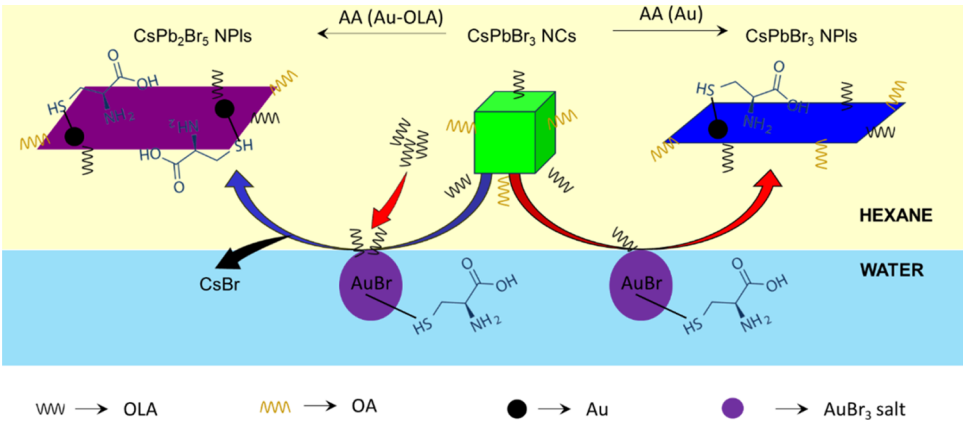

Figure 6. Schematic summary of the AA cysteine-driven reaction mechanism at the water-hexane interface. At first, the colloidal hexane solution of $CsPbBr_3$ PNCs is treated with $AuBr_3$ and cysteine-saturated aqueous solution, i.e., with Au-cysteine thiolate complex. The OLA ligand shuttles the Au-cysteine thiolate complex from the aqueous to the hexane phase where $CsPbBr_3$ PNCs reside, leading to the formation of 2D $CsPbBr_3$ NPls by preferential binding of the Au-cysteine thiolate complex to a specific crystal facet. With excess of the OLA molecules and prolonged reaction time, further chemical transformation to 2D $CsPb_2Br_5$ NPls takes place via simultaneous Au-cysteine thiolate complex shuttling and CsBr stripping in hexane and water, respectively.

presence of AA cysteine in the product (Figure 4b). Importantly, the core-level XPS spectra of Au $4f_{7/2}$ and $4f_{5/2}$ appear to be asymmetric in shape, and the Gaussian fitting results in two peaks responsible for each Au 4f spectra (Figure 4b). While the lower-binding-energy peaks at 83.9 and 87.6 eV are responsible for metallic Au (0), the higher-binding-energy peaks at 84.7 and 88.5 eV can be associated with the Au atom bonded to the S atom of cysteine (i.e., Au−S bond).[51] Similarly, the core-level XPS spectra of Pb $4f_{7/2}$ and $4f_{5/2}$ show additional higher-binding-energy peaks at 140 and 144.6 eV along with the main 4f peaks at lower binding energy (Figure 3bi) and might be associated with Pb−S bonding. Thus, the FTIR and XPS results conclusively indicate that the S atoms are covalently bonded to the Au and Pb atoms on the surface of PNCs, and that the phase transition is triggered by the AA cysteine itself.

https://doi.org/10.1021/acsomega.4c04364
ACS Omega 2024, 9, 31026−31034

The TEM images of the untreated and AA-treated $CsPbBr_3$ PNCs are shown in Figure 5. As shown in Figure 5a, the TEM image of the untreated $CsPbBr_3$ PNCs shows a typical cubic morphology and size of ∼13 nm. The TEM images and size distribution of the AA (Au)-treated PNCs (Figures 5b,c and S4) show nanoplatelets of dimensions 30 nm × 4.5 nm. Interestingly, the HRTEM images of the selected region of the corresponding sample in Figure 5b show a unique arrangement of NPls decorated with dark black particles. The I-FFT analysis of the NPls reveals a lattice spacing of 0.57 nm, corresponding to the (100) plane of the $CsPbBr_3$ crystal. The dark black particles, however, are attributed to Au particles.[42] This observation evidently supports that on treatment with AA (Au), the cubic $CsPbBr_3$ PNCs transform into $CsPbBr_3$ NPls.

In contrast, the TEM images of the AA (Au-OLA)-treated PNCs in Figures 5d and S4 show an irregular morphology of nanoribbons and nanoplates, which we identified as transformation to $CsPb_2Br_5$ NPls. Although the obtained $CsPb_2Br_5$ NPls show a somewhat irregular morphology, the optical spectra are quite robust, as shown in Figure 2c,d. The formation of $CsPb_2Br_5$ NPls is further corroborated by the HRTEM analysis, which reveals a lattice spacing of 0.268 nm, corresponding to the (312) plane of the $CsPb_2Br_5$ phase.[47] The corresponding size distribution analysis suggests that the dimensions of the obtained NPls are 66 nm × 16 nm (Figure 5e). Similar to the AA (Au)-treated PNCs, the AA (Au-OLA)-treated PNCs show dark black Au particles on top of the $CsPb_2Br_5$ nanoplates, which, when analyzed by HRTEM measurement, provides a lattice spacing of 0.23 nm, indicating the (111) plane of Au (Figure 5dii).[42]

The mechanistic details of the chemical transformation of the cubic $CsPbBr_3$ PNCs to different morphologies/phases caused by AA (Au) or AA (Au-OLA) treatment are schematically depicted in Figure 6. As the ligand, OLA alone, is not able to shuttle AA cysteine from water to the hexane phase, we use $AuBr_3$ as a mediator to execute the shuttling. In the aqueous solution, $AuBr_3$ and cysteine form a complex, called Au-cysteine thiolate,[52] to which $CsPbBr_3$ PNCs-enriched hexane solution is added. Subsequently, the excess OLA ligands travel to the interface, coordinate with the Au atom in the Au-cysteine thiolate complex, and shuttle into the hexane phase. Finally, the Au-cysteine thiolate complex interacts with the $CsPbBr_3$ PNCs and transforms into $CsPbBr_3$ NPls. The formation of the Au-cysteine thiolate complex can be substantiated from the XPS measurement, where clearly Au−S bond formation has been observed, which eventually integrates into the perovskite surface upon chemical transformation. Further, the S atom is also covalently bonded to the surface Pb atoms of the perovskite, as confirmed by FTIR and XPS results, directing the AA cysteine to be indeed present in the products. In addition, we believe possibly both the amine and carboxyl group of the Au-cysteine thiolate complex bind the perovskite surface to a specific facet, leading to restricted growth in the corresponding direction only and subsequent formation of the anisotropic 2D $CsPbBr_3$ NPls. This idea can be further substantiated by the recent report of the Bawendi group showing preferential binding of S-based zwitterionic ligands to specific crystal facets of perovskite, leading to the formation of corresponding NPls.[53] It is important to note that earlier studies showed that the inhomogeneous distribution of amino acids in oxide semiconductors introduced a quantum confinement effect, resulting in a blue shift in the optical spectra,[16,18] which is different from the present study. Moreover, at the same time, the Au particles are deposited on the perovskite surface, resulting in the formation of Au-decorated $CsPbBr_3$ NPls.

Upon addition of excess OLA molecules, the shuttling of the Au-cysteine thiolate complex accelerates drastically, leading to an enhanced interaction of PNCs with the aqueous solution. Importantly, prolonging the reaction time for 24−48 h not only leads to enhanced interaction of the Au-cysteine thiolate complex with the $CsPbBr_3$ PNCs but also increases interaction with the aqueous solution. As mentioned in the Introduction section, $CsPbBr_3$ PNCs are highly ionic lattices; therefore, prolonged interaction with water promotes the stripping of the ionic CsBr salt to the water.[9] This has been further verified by measuring the XRD pattern of the white precipitated powder obtained after the reaction with the AA (Au-OLA)-treated $CsPbBr_3$ PNCs, where some of the XRD peaks showing CsBr characteristics (Figure S5). In effect, simultaneous dimensional reduction via preferential binding to specific perovskite facets and phase transformation to 2D $CsPb_2Br_5$ NPls take place.

CONCLUSIONS

We showed that AA cysteine functionalization in the cubic $CsPbBr_3$ PNCs via water-hexane interfacial chemistry leads to chemical transformation to $CsPbBr_3$ NPls, and subsequently to $CsPb_2Br_5$ NPls. To facilitate the chemical transformation, $AuBr_3$ salts are added into an aqueous solution that forms the Au-cysteine thiolate complex, which travels from water to the hexane phase via the shuttling ligand OLA to initiate the reaction with $CsPbBr_3$ PNCs. The reaction dynamics is probed using optical spectroscopy, clearly revealing the formation of $CsPbBr_3$ NPls. On adding excess OLA molecules and prolonging the reaction time, it leads to the formation of $CsPb_2Br_5$ NPls, as evidenced by the corresponding blue-shifted optical spectra. Further measurements, including XRD, XPS, FTIR, TEM, and HRTEM, suggest the formation of Au-decorated 2D $CsPbBr_3$ and $CsPb_2Br_5$ NPls. We finally provided mechanistic insights on the dimensional reduction and phase transformation using Au-cysteine thiolate complex shuttling into hexane and ionic CsBr stripping into water. We believe the interfacial chemistry of AA functionalization of perovskite NCs may open a new avenue to control the optical properties in the nanoscale.

EXPERIMENTAL METHODS

1.1. Materials. Cesium carbonate ($CsCO_3$), lead bromide ($PbBr_2$), 1-octadecene (ODE), oleic acid (OA), oleylamine (OLA), L-cysteine, and hexane were obtained from Sigma-Aldrich.

1.2. Preparation of Untreated $CsPbBr_3$ PNCs. *Cesium-Oleate Stock Solution.* 133 mg (0.4 mmol) of Cs_2CO_3 was taken in 10 mL of octadecene (ODE) with 1 mL of oleic acid (OA) in a 30 mL glass vial and heated to 120 °C, which led to obtaining a clear transparent solution, implying the formation of the Cs-oleate stock solution. This solution was then kept at 160 °C.

Hot-Injection Synthesis. A 69 mg portion (0.188 mmol) of $PbBr_2$ was taken in 5 mL of an ODE with 0.5 mL of OA and 0.5 mL of oleylamine (OLA) in a 30 mL glass vial, heated to 120 °C, and kept for some time until we obtained a clear transparent solution. The temperature was then ramped up to 175 °C and 0.4 mL of the Cs-oleate stock solution was injected into this solution. The reaction mixture was then immediately

https://doi.org/10.1021/acsomega.4c04364
ACS Omega 2024, 9, 31026−31034

quenched in ice-cold water, centrifuged at 10,000 rpm, redispersed in 1 mL of hexane, and recentrifuged at 6000 rpm. The supernatant was then collected and redispersed in hexane, which contains the monodisperse $CsPbBr_3$ nanocrystals, for further use.

1.3. Amino Acid Cysteine Incorporation into $CsPbBr_3$ NCs. *Cysteine Stock Solution.* 40 mg of L-cysteine was dissolved in 0.13 mL of milli-Q water to obtain the saturated cysteine stock solution. The dissolution was performed by taking the solution in a 2 mL Eppendorf and vortexing it.

Gold (Au) Stock Solution. 10 mg of $AuBr_3$ was dissolved in 0.08 mL of milli-Q water to obtain the saturated Au stock solution. The dissolution was performed by taking the solution in a 2 mL Eppendorf and vortexing it.

OLA Stock Solution. A 0.01 mL portion of the OLA was dissolved in 2 mL of hexane to obtain the OLA stock solution. The dissolution was performed by taking the solution in a 2 mL Eppendorf and vortexing it.

AA-Treated $CsPbBr_3$ PNCs. 0.04 mL of the cysteine stock solution was taken with 0.4 mL of the OLA stock solution in a 2 mL Eppendorf and vortexed for 5 min. The solution was then kept for about 5 min to settle down, and the water and hexane phases to separate. The clear upper hexane phase of the mixture was taken and added to 0.15 mL of $CsPbBr_3$ kept in another 2 mL Eppendorf and vortexed. This solution was kept for 48 h before performing any measurements on it.

AA (Au)-Treated $CsPbBr_3$ PNCs. A 0.2 mL portion of the $CsPbBr_3$ was taken in a 2 mL Eppendorf tube, and 0.3 mL of hexane was added to it to dilute the solution. 0.02 mL of cysteine stock and 0.02 mL of Au stock solution were added to it, and the mixture was vortexed for 1 min. The solution was then kept for about 5 min to settle down; the water and hexane phases separated, with a deposition of white powdery precipitate. The upper hexane phase was extracted and kept in another 2 mL Eppendorf. This solution was kept for 48 h before performing any measurements on it.

AA (Au-OLA)-Treated $CsPbBr_3$ PNCs. 0.2 mL of the $CsPbBr_3$ was taken in a 2 mL Eppendorf and 0.3 mL of the OLA stock solution was added to it. 0.02 mL of cysteine stock and 0.02 mL of Au stock solution were added to it and the mixture was vortexed for 1 min. The solution was then kept for about 5 min to settle down; the water and hexane phase separated, with a deposition of white powdery precipitate. The hexane phase, which was a little dirty brownish, was extracted and kept in another 2 mL Eppendorf. This solution was kept for 48 h before performing any measurements on it.

■ ASSOCIATED CONTENT

Supporting Information

The Supporting Information is available free of charge at https://pubs.acs.org/doi/10.1021/acsomega.4c04364.

Further data on absorption, PL spectra, XRD and TEM images (PDF)

■ AUTHOR INFORMATION

Corresponding Author

Tushar Debnath − *Centre for Nanotechnology, Indian Institute of Technology Guwahati, Guwahati 781039 Assam, India; Nano Physical Spectroscopy Group, Department of Chemistry, School of Natural Sciences, Shiv Nadar Institution of Eminence, Delhi NCR 201314 Uttar Pradesh, India;* orcid.org/0000-0002-8108-4482; Email: tushar.debnath@snu.edu.in, debnathtushar@gmail.com

Authors

Nikunj Agarwal − *Centre for Nanotechnology, Indian Institute of Technology Guwahati, Guwahati 781039 Assam, India*

Deepshikha Agarwal − *Centre for Nanotechnology, Indian Institute of Technology Guwahati, Guwahati 781039 Assam, India*

Complete contact information is available at: https://pubs.acs.org/10.1021/acsomega.4c04364

Author Contributions

[§]N.A. and D.A. contributed equally to this work.

Notes

The authors declare no competing financial interest.

■ ACKNOWLEDGMENTS

T.D. acknowledges the Department of Science & Technology (DST) and the Science and Engineering Research Board (SERB) for the Ramanujan Fellowship Award (RJF/2021/000125) and the Core Research Grant (CRG/2023/000519). The authors thank the Centre for Nanotechnology, Department of Chemistry and Central Instrumental Facility, IIT Guwahati, for instrument support. They also sincerely thank Prof. A. Chattopadhyay, IIT Guwahati for his help and encouragement, and for providing the lab facility.

■ REFERENCES

(1) García de Arquer, F. P.; Talapin, D. V.; Klimov, V. I.; Arakawa, Y.; Bayer, M.; Sargent, E. H. Semiconductor Quantum Dots: Technological Progress and Future Challenges. *Science* **2021**, *373*, No. eaaz8541.

(2) Liu, M.; Yazdani, N.; Yarema, M.; Jansen, M.; Wood, V.; Sargent, E. H. Colloidal Quantum Dot Electronics. *Nat. Electron.* **2021**, *4*, 548−558.

(3) Ohtomo, A.; Kawasaki, M.; Koida, T.; Masubuchi, K.; Koinuma, H.; Sakurai, Y.; Yoshida, Y.; Yasuda, T.; Segawa, Y. Mgxzn1−Xo as a Ii−Vi Widegap Semiconductor Alloy. *Appl. Phys. Lett.* **1998**, *72*, 2466−2468.

(4) Mocatta, D.; Cohen, G.; Schattner, J.; Millo, O.; Rabani, E.; Banin, U. Heavily Doped Semiconductor Nanocrystal Quantum Dots. *Science* **2011**, *332*, 77−81.

(5) Pradhan, N.; Sarma, D. D. Advances in Light-Emitting Doped Semiconductor Nanocrystals. *J. Phys. Chem. Lett.* **2011**, *2*, 2818−2826.

(6) Sichert, J. A.; et al. Quantum Size Effect in Organometal Halide Perovskite Nanoplatelets. *Nano Lett.* **2015**, *15*, 6521−6527.

(7) Otero-Martínez, C.; García-Lojo, D.; Pastoriza-Santos, I.; Pérez-Juste, J.; Polavarapu, L. Dimensionality Control of Inorganic and Hybrid Perovskite Nanocrystals by Reaction Temperature: From No-Confinement to 3d and 1d Quantum Confinement. *Angew. Chem. In. Ed.* **2021**, *60*, 26677−26684.

(8) Lei, B.; et al. Direct Observation of Semiconductor−Metal Phase Transition in Bilayer Tungsten Diselenide Induced by Potassium Surface Functionalization. *ACS Nano* **2018**, *12*, 2070−2077.

(9) Wu, L.; et al. From Nonluminescent Cs4pbx6 (X = Cl, Br, I) Nanocrystals to Highly Luminescent Cspbx3 Nanocrystals: Water-Triggered Transformation through a Csx-Stripping Mechanism. *Nano Lett.* **2017**, *17*, 5799−5804.

(10) Borukhin, S.; Bloch, L.; Radlauer, T.; Hill, A. H.; Fitch, A. N.; Pokroy, B. Screening the Incorporation of Amino Acids into an Inorganic Crystalline Host: The Case of Calcite. *Adv. Funct. Mater.* **2012**, *22*, 4216−4224.

(11) Green, D. C.; Darkins, R.; Marzec, B.; Holden, M. A.; Ford, I. J.; Botchway, S. W.; Kahr, B.; Duffy, D. M.; Meldrum, F. C. Dichroic

Calcite Reveals the Pathway from Additive Binding to Occlusion. *Cryst. Growth Des.* **2021**, *21*, 3746−3755.
(12) Nahi, O.; Kulak, A. N.; Kress, T.; Kim, Y.-Y.; Grendal, O. G.; Duer, M. J.; Cayre, O. J.; Meldrum, F. C. Incorporation of Nanogels within Calcite Single Crystals for the Storage, Protection and Controlled Release of Active Compounds. *Chem. Sci.* **2021**, *12*, 9839−9850.
(13) Kim, Y.-Y.; et al. Tuning Hardness in Calcite by Incorporation of Amino Acids. *Nat. Mater.* **2016**, *15*, 903−910.
(14) Brif, A.; Bloch, L.; Pokroy, B. Bio-Inspired Engineering of a Zinc Oxide/Amino Acid Composite: Synchrotron Microstructure Study. *CrystEngComm* **2014**, *16*, 3268−3273.
(15) Brif, A.; Ankonina, G.; Drathen, C.; Pokroy, B. Bio-Inspired Band Gap Engineering of Zinc Oxide by Intracrystalline Incorporation of Amino Acids. *Adv. Mater.* **2014**, *26*, 477−481.
(16) Muhammed, M. A. H.; et al. Strong Quantum Confinement Effects and Chiral Excitons in Bio-Inspired Zno−Amino Acid Cocrystals. *J. Phys. Chem. C* **2018**, *122*, 6348−6356.
(17) Polishchuk, I.; Bianco-Stein, N.; Lang, A.; Kurashvili, M.; Toroker, M. C.; Katsman, A.; Feldmann, J.; Pokroy, B. Strong Band Gap Blueshift in Copper (I) Oxide Semiconductor Via Bioinspired Route. *Adv. Funct. Mater.* **2020**, *30*, No. 1910405.
(18) Kurashvili, M.; Polishchuk, I.; Lang, A.; Strohmair, S.; Richter, A. F.; Rieger, S.; Debnath, T.; Pokroy, B.; Feldmann, J. Disorder and Confinement Effects to Tune the Optical Properties of Amino Acid Doped Cu2o Crystals. *Adv. Funct. Mater.* **2022**, *32*, No. 2202121.
(19) Lang, A.; Polishchuk, I.; Seknazi, E.; Feldmann, J.; Katsman, A.; Pokroy, B. Bioinspired Molecular Bridging in a Hybrid Perovskite Leads to Enhanced Stability and Tunable Properties. *Adv. Funct. Mater.* **2020**, *30*, No. 2005136.
(20) Ghosh, S.; Kar, P. Aromatic Amino Acid-Mediated Perovskite Nanocrystals: Fluorescence Tuning and Morphological Evolution. *Inorg. Chem.* **2022**, *61*, 10079−10088.
(21) Zhang, W.; Du, J.; Zhang, W.; Chu, Y.; Mei, A.; Rong, Y.; Gao, X.; Han, H.; Hu, Y. Unveiling the Effect of Amino Acids on the Crystallization Pathways of Methylammonium Lead Iodide Perovskites. *J. Energy Chem.* **2022**, *69*, 253−260.
(22) Dey, A.; et al. State of the Art and Prospects for Halide Perovskite Nanocrystals. *ACS Nano* **2021**, *15*, 10775−10981.
(23) Akkerman, Q. A.; D'Innocenzo, V.; Accornero, S.; Scarpellini, A.; Petrozza, A.; Prato, M.; Manna, L. Tuning the Optical Properties of Cesium Lead Halide Perovskite Nanocrystals by Anion Exchange Reactions. *J. Am. Chem. Soc.* **2015**, *137*, 10276−10281.
(24) Protesescu, L.; Yakunin, S.; Bodnarchuk, M. I.; Krieg, F.; Caputo, R.; Hendon, C. H.; Yang, R. X.; Walsh, A.; Kovalenko, M. V. Nanocrystals of Cesium Lead Halide Perovskites ($CsPbBr_3$, X = Cl, Br, and I): Novel Optoelectronic Materials Showing Bright Emission with Wide Color Gamut. *Nano Lett.* **2015**, *15*, 3692−3696.
(25) Shamsi, J.; Urban, A. S.; Imran, M.; De Trizio, L.; Manna, L. Metal Halide Perovskite Nanocrystals: Synthesis, Post-Synthesis Modifications, and Their Optical Properties. *Chem. Rev.* **2019**, *119*, 3296−3348.
(26) López-Fernández, I.; et al. Lead-Free Halide Perovskite Materials and Optoelectronic Devices: Progress and Prospective. *Adv. Funct. Mater.* **2024**, *34*, No. 2307896.
(27) Mourdikoudis, S.; Menelaou, M.; Fiuza-Maneiro, N.; Zheng, G.; Wei, S.; Pérez-Juste, J.; Polavarapu, L.; Sofer, Z. Oleic Acid/Oleylamine Ligand Pair: A Versatile Combination in the Synthesis of Colloidal Nanoparticles. *Nanoscale Horiz.* **2022**, *7*, 941−1015.
(28) Fiuza-Maneiro, N.; Sun, K.; López-Fernández, I.; Gómez-Graña, S.; Müller-Buschbaum, P.; Polavarapu, L. Ligand Chemistry of Inorganic Lead Halide Perovskite Nanocrystals. *ACS Energy Lett.* **2023**, *8*, 1152−1191.
(29) Akkerman, Q. A.; et al. Controlling the Nucleation and Growth Kinetics of Lead Halide Perovskite Quantum Dots. *Science* **2022**, *377*, 1406−1412.
(30) Manna, M.; Pal, S.; Goswami, T.; Bhandari, S.; Debnath, T. Halide-Driven Halogen−Hydrogen Bonding Versus Chelation in Perovskite Nanocrystals: A Concept of Charge Transfer Bridging. *J. Phys. Chem. Lett.* **2023**, *14*, 354−362.
(31) DuBose, J. T.; Kamat, P. V. Energy Versus Electron Transfer: Managing Excited-State Interactions in Perovskite Nanocrystal−Molecular Hybrids. *Chem. Rev.* **2022**, *122*, 12475−12494.
(32) DuBose, J. T.; Kamat, P. V. Probing Perovskite Photocatalysis. Interfacial Electron Transfer between $CsPbBr_3$ and Ferrocene Redox Couple. *J. Phys. Chem. Lett.* **2019**, *10*, 6074−6080.
(33) Maity, P.; Dana, J.; Ghosh, H. N. Multiple Charge Transfer Dynamics in Colloidal Cspbbr3 Perovskite Quantum Dots Sensitized Molecular Adsorbate. *J. Phys. Chem. C* **2016**, *120*, 18348−18354.
(34) Balakrishnan, S. K.; Kamat, P. V. Ligand Assisted Transformation of Cubic Cspbbr3 Nanocrystals into Two-Dimensional Cspb2br5 Nanosheets. *Chem. Mater.* **2018**, *30*, 74−78.
(35) Paul, S.; et al. Manganese-Doping-Induced Quantum Confinement within Host Perovskite Nanocrystals through Ruddlesden-Popper Defects. *Angew. Chem., Int. Ed.* **2020**, *59*, 6794−6799.
(36) Turedi, B.; Lee, K. J.; Dursun, I.; Alamer, B.; Wu, Z.; Alarousu, E.; Mohammed, O. F.; Cho, N.; Bakr, O. M. Water-Induced Dimensionality Reduction in Metal-Halide Perovskites. *J. Phys. Chem. C* **2018**, *122*, 14128−14134.
(37) Hu, H.; Wu, L.; Tan, Y.; Zhong, Q.; Chen, M.; Qiu, Y.; Yang, D.; Sun, B.; Zhang, Q.; Yin, Y. Interfacial Synthesis of Highly Stable CsPbX3/Oxide Janus Nanoparticles. *J. Am. Chem. Soc.* **2018**, *140*, 406−412.
(38) Pramanik, A.; Patibandla, S.; Gao, Y.; Gates, K.; Ray, P. C. Water Triggered Synthesis of Highly Stable and Biocompatible 1D Nanowire, 2D Nanoplatelet, and 3D Nanocube CsPbBr3 Perovskites for Multicolor Two-Photon Cell Imaging. *JACS Au* **2021**, *1*, 53−65.
(39) Das, A.; Debnath, T. Water-Triggered Chemical Transformation of Perovskite Nanocrystals. *Chem. - Eur. J.* **2023**, *29*, No. e202202475.
(40) Wu, L.; Wang, Y.; Kurashvili, M.; Dey, A.; Cao, M.; Döblinger, M.; Zhang, Q.; Feldmann, J.; Huang, H.; Debnath, T. Interfacial Manganese-Doping in CsPbBr3 Nanoplatelets by Employing a Molecular Shuttle. *Angew. Chem. In. Ed.* **2022**, *61*, No. e202115852.
(41) Das, A.; Debnath, T. Giant Exciton Stokes Shift in Interfacially Prepared Cs(Mn/Pb)Cl3 Alloy Nanoplatelets. *J. Phys. Chem. Lett.* **2023**, *14*, 5940−5948.
(42) Samanta, S.; Paul, S.; Debnath, T. Obtaining Ligand-Free Aqueous Au-Nanoparticles Using Reversible CsPbBr3 ↔ Au@CsPbBr3 Nanocrystal Transformation. *Small* **2024**, No. 2311712.
(43) Bohn, B. J.; et al. Boosting Tunable Blue Luminescence of Halide Perovskite Nanoplatelets through Postsynthetic Surface Trap Repair. *Nano Lett.* **2018**, *18*, 5231−5238.
(44) Mir, W. J.; Jagadeeswararao, M.; Das, S.; Nag, A. Colloidal Mn-Doped Cesium Lead Halide Perovskite Nanoplatelets. *ACS Energy Lett.* **2017**, *2*, 537−543.
(45) Krajewska, C. J.; Kaplan, A. E. K.; Kick, M.; Berkinsky, D. B.; Zhu, H.; Sverko, T.; Van Voorhis, T.; Bawendi, M. G. Controlled Assembly and Anomalous Thermal Expansion of Ultrathin Cesium Lead Bromide Nanoplatelets. *Nano Lett.* **2023**, *23*, 2148−2157.
(46) Li, J.; Zhang, H.; Wang, S.; Long, D.; Li, M.; Guo, Y.; Zhong, Z.; Wu, K.; Wang, D.; Zhang, T. Synthesis of All-Inorganic Cspb2br5 Perovskite and Determination of Its Luminescence Mechanism. *RSC Adv.* **2017**, *7*, 54002−54007.
(47) Acharyya, P.; Pal, P.; Samanta, P. K.; Sarkar, A.; Pati, S. K.; Biswas, K. Single Pot Synthesis of Indirect Band Gap 2D CsPb2Br5 Nanosheets from Direct Band Gap 3D CsPbBr3 Nanocrystals and the Origin of Their Luminescence Properties. *Nanoscale* **2019**, *11*, 4001−4007.
(48) Sahu, S.; Debnath, T.; Sahu, K. Reversible CsPbBr3 ↔ CsPb2Br5 Transformation Via Reverse Micellar Aqueous Solution. *J. Phys. Chem. Lett.* **2024**, *15*, 3677−3682.
(49) Akkerman, Q. A.; et al. Solution Synthesis Approach to Colloidal Cesium Lead Halide Perovskite Nanoplatelets with Monolayer-Level Thickness Control. *J. Am. Chem. Soc.* **2016**, *138*, 1010−1016.

https://doi.org/10.1021/acsomega.4c04364
ACS Omega 2024, 9, 31026−31034

(50) Li, L.; Liao, L.; Ding, Y.; Zeng, H. Dithizone-Etched CdTe Nanoparticles-Based Fluorescence Sensor for the Off−on Detection of Cadmium Ion in Aqueous Media. *RSC Adv.* **2017**, *7*, 10361−10368.
(51) Vitale, F.; Fratoddi, I.; Battocchio, C.; Piscopiello, E.; Tapfer, L.; Russo, M. V.; Polzonetti, G.; Giannini, G. Mono-and bi-functional arenethiols as surfactants for gold nanoparticles: synthesis and characterization. *Nanoscale Res. Lett.* **2011**, *6*, No. 103.
(52) Nie, H. Y.; Romanovskaia, E.; Romanovski, V.; Hedberg, J.; Hedberg, Y. S. Detection of Gold Cysteine Thiolate Complexes on Gold Nanoparticles with Time-of-Flight Secondary Ion Mass Spectrometry. *Biointerphases* **2021**, *16*, No. 021005.
(53) Zhu, H.; Kick, M.; Ginterseder, M.; Krajewska, C. J.; Šverko, T.; Li, R.; Lu, Y.; Shih, M.-C.; Van Voorhis, T.; Bawendi, M. G. Synthesis of Zwitterionic CsPbBr3 Nanocrystals with Controlled Anisotropy Using Surface-Selective Ligand Pairs. *Adv. Mater.* **2023**, *35*, No. 2304069.

https://doi.org/10.1021/acsomega.4c04364
ACS Omega 2024, 9, 31026−31034